RSC Applied Interfaces

Accepted Manuscript

This article can be cited before page numbers have been issued, to do this please use: K. Kawaai, N. Ota, S. Arai, M. Yamamoto, T. Tanabe and T. Yoshida, *RSC Appl. Interfaces*, 2026, DOI: 10.1039/D6LF00085A.

ROYAL SOCIETY OF CHEMISTRY

rsc.li/RSCApplInter

View Article Online
DOI: 10.1039/D6LF00085A

ARTICLE

Photocatalytic reduction of CO_2 with water using catalysts of γ-Ga_2O_3 supported by α-Ga_2O_3 : mechanism and roles of each phase

Received 00th January 20xx,
Accepted 00th January 20xx

DOI: 10.1039/x0xx00000x

Kosuke Kawaai [a], Naoto Ota [b], Shigeo Arai [c], Muneaki Yamamoto [c], Tetsuo Tanabe [a], Tomoko Yoshida *[a]

Gallium oxide (Ga_2O_3) consisting of the mixed phases of α and β, β and γ, and α and γ is known as a photocatalyst for the reduction of CO_2 with water producing CO, H_2 and O_2. In previous studies, we have investigated Ga_2O_3 consisting of the mixed phases of α-Ga_2O_3 and γ-Ga_2O_3 systematically varying the contents of γ-Ga_2O_3 as catalysts for the photoreduction of CO_2 with water, and proposed a crude reaction mechanism of the photocatalytic reduction of CO_2. However, the mechanism should be refined to clarify the roles of each phase and effects morphology of the mixture. To do this, we have investigated the photocatalytic activity of γ-Ga_2O_3 supported by α-Ga_2O_3 instead of their mixed phases previously examined. With increasing the contents of γ-Ga_2O_3, H_2 production rates monotonically decreased, whereas CO production rates increased, reached a maximum at 60%-80% of the γ-Ga_2O_3 content, and decreased significantly. These trends are consistent with those observed in the previous studies using the mixed phases. Based on the previously suggested mechanism, we have proposed the detailed mechanism as follows : (1) the surfaces of α-Ga_2O_3 and γ-Ga_2O_3 particles are hydro-oxidated to GaOOH in water and GaOOH on the γ-Ga_2O_3 particles absorbs CO_2 as bicarbonate , (2) GaOOH on α-Ga_2O_3 is photo-decomposed to α-Ga_2O_3 producing H, (3) the produced H migrates to the γ-Ga_2O_3 particles and reuces the adsorbed bocarbonate to CO, and (4) without UV-photon, the surfaces of α-Ga_2O_3 and γ-Ga_2O_3 return to their initial states of GaOOH and bicarbonate absorbing state, respectively.

Introduction

Ga_2O_3 is well known as a photocatalyst for CO_2 reduction with water. Among its several different crystalline phases, either α, β, or γ phase has been used in most of the previous studies. In order to increase the production rate and selectivity of CO among CO_2 reduction products, metallic cocatalysts such as Ag [1-5] and others [6-8] have often been employed. In our previous works, it has been shown that mixed phases of α and β [9], α and γ [10], and β and γ [11] exhibit high photocatalytic activity without the co-catalysts.

In a previous work [10], making detailed investigation of the mixed phases of α-Ga_2O_3 and γ-Ga_2O_3 as the photocatalyst of the CO_2 reduction with water, we have suggested the CO_2 reduction mechanism such that water splitting dominates on α-Ga_2O_3 and its product of H reduces CO_2 adsorbed on the γ-Ga_2O_3 to CO. However, in the mixed phases of α-Ga_2O_3 and γ-Ga_2O_3, it was difficult to control the morphology of the mixture and the particle sizes of both phases.

In order to verify the mechanism, we have investigated the catalytic activity of γ-Ga_2O_3 supported by α-Ga_2O_3 for the photocatalytic CO_2 reduction with water instead of the mixed phases of α-Ga_2O_3 and γ-Ga_2O_3 previously examined. The supported catalysts made it easier to control the contents and morphology of the γ-Ga_2O_3 with clear separation of the γ-Ga_2O_3 and α-Ga_2O_3. Comparing the present results with the previous ones obtained using the mixed phases of α-Ga_2O_3 and γ-Ga_2O_3, we have confirmed the previously suggested CO_2 reduction mechanism is basically correct and given improved one. Furthermore, the roles of each phase in the mixed phase samples of the previous work and the present supported samples have been clarified

Experimental

Experimental Procedures

γ-Ga_2O_3 supported by α-Ga_2O_3 photocatalysts (referred to as γ-Ga_2O_3/α-Ga_2O_3 hereafter) were synthesized by an impregnation method. Their γ-Ga_2O_3 contents were determined by XAFS analysis and their morphology (geometrical structure) was observed by a transmission electron microscope (TEM). Specific surface area was measured by the BET method. CO_2 adsorption on γ-Ga_2O_3/α-Ga_2O_3 was also examined by temperature programmed desorption (TPD). The photocatalytic CO_2 reduction with water under UV light illumination was carried out and analyzed in terms of the γ-Ga_2O_3 content, the morphology, and the specific surface area.

Catalysts preparation

[a] Department of Energy Engineering, Graduate School of Engineering, Nagoya University, Furo-cho, Chikusa-ku, Nagoya 464-8603, Japan E-mail: tyoshida@energy.nagoya-u.ac.jp; Tel: +81-52-789-5935
[b] Department of Applied Chemistry and Bioengineering, Graduate School of Engineering, Osaka Metropolitan University, Sugimoto 3-3 138, Sumiyoshiku-ku, Osaka 558-8585, Japan
[c] Institute of Materials and Systems for Sustainability, Nagoya University, Furo-cho, Chikusa-ku, Nagoya 464-8603, Japan

View Article Online
DOI: 10.1039/D6LF00085A

At first, $Ga(NO_3)_3 \cdot 8H_2O$ (KISHIDA Chemical Corporation, purity 99%) was dissolved in distilled water. Then, α-Ga_2O_3 powders, prepared by the calcination of GaOOH at 450℃ for 4h as reported by Li *et al.* [12], were dispersed in the solution. The dispersed solution was dried up and calcined at 450℃ for 4 h in air resulting in γ-Ga_2O_3/α-Ga_2O_3 samples. The contents of γ-Ga_2O_3 (the γ-Ga_2O_3 contents) in γ-Ga_2O_3/α-Ga_2O_3 (nominal contents) were controlled by varying the amounts of $Ga(NO_3)_3 \cdot 8H_2O$ and α-Ga_2O_3.

Photocatalytic CO_2 reduction with water under UV light irradiation

A sample (0.1 g) was dispersed in water of 100 mL with 0.5 M $NaHCO_3$ and stirred in a reaction cell made of quartz. CO_2 gas was flowed into the reaction cell with 3 mL/min. The UV light was given by a Xe lamp through a UV cold mirror. The intensity of the light was 35 mW/cm^2 at 254±10 nm. The produced gases (mostly H_2, CO, and O_2) were quantified by a gas chromatograph (TCD-GC, Shimadzu GC 8A). The reactions were monitored over five hours to confirm the steady state production rates of H_2 and CO which were determined every one hour.

Characterization

The morphology of the samples was observed by TEM and their specific surface areas were determined by the BET method. Their crystalline structures were determined by an X-ray diffraction (XRD) analysis. X-ray absorption analyses (XANES/EXAFS) were also employed and used to determine the γ-Ga_2O_3 contents of the samples.

TEM images were observed with JEM-1000K RS (JEOL Ltd.) under an acceleration voltage of 1000 kV at the High Voltage Electron Microscope Laboratory in Nagoya University. XRD patterns were recorded on Rigaku MiniFlex 600 (Cu Kα radiation, 40kV, 15mA) at room temperature. Ga K-edge XANES/EXAFS spectra were measured by the transmission method at room temperature at the beam line of 5S1 and 11S2 at Aichi Synchrotron Radiation Center. The ionization chambers were filled with 100% N_2 for incident X-rays (I_0) and 50% N_2 and 50% Ar for transmitted X-rays (I). Powder samples were set on a masking tape to be thick enough to measure XANES/EXAFS. Specific surface areas were determined by the BET method with N_2 adsorption at -196℃ using a Monosorb™ (Quantachrome). Samples were outgassed at 300℃ for 30 min under N_2 gas flow before measurement. FT-IR spectra were recorded with FT/IR-6100 (JASCO Co.) in the transmission mode at room temperature. Before the measurement, the sample was heated at 400℃ for 1h. Temperature programmed desorption of CO_2 (CO_2-TPD) was carried out as follows. After drying the sample (50 mg) under He gas flow (50 mL/min) at 400 ℃ for 1 h, CO_2 was adsorbed under pure CO_2 gas flow at 40 ℃ for 1h. Changing the CO_2 gas flow to the He gas flow (30 mL/min), CO_2 desorption profiles of the samples were measured changing the

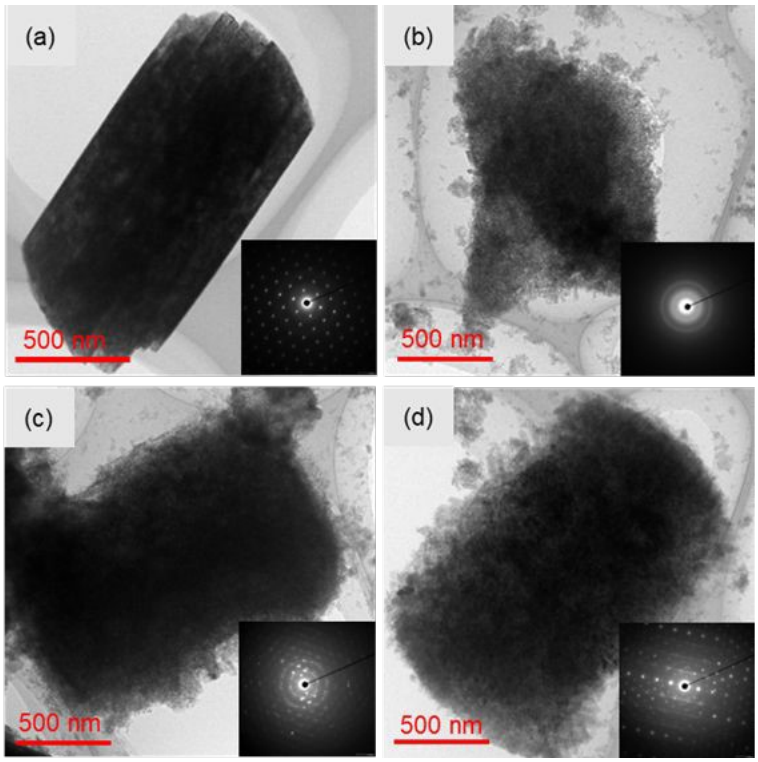

Fig. 1 TEM images and electron diffraction patterns of (a) α-Ga_2O_3 (b) γ-Ga_2O_3 (c) γ-Ga_2O_3/α-Ga_2O_3 (γ=30%) (d) γ-Ga_2O_3/α-Ga_2O_3 (γ=60%)

View Article Online
DOI: 10.1039/D6LF00085A

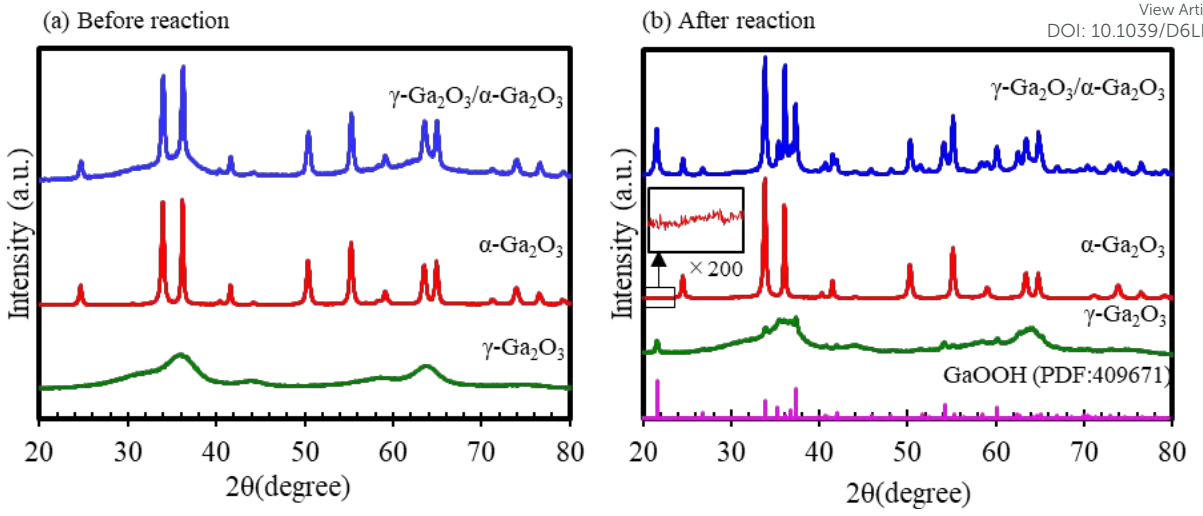

Fig. 2 XRD patterns of γ-Ga_2O_3/α-Ga_2O_3, α-Ga_2O_3, and γ-Ga_2O_3 before(a) and after(b) the reaction. The inset is an enlarged view of lower angle side of the α-Ga_2O_3 spectrum to show the appearance of GaOOH

temperature from 40 °C to 600 °C with the heating rate of 10 °C/min.

Results

TEM

Fig. 1 shows the TEM images and the electron diffraction patterns of α-Ga_2O_3 (a), γ-Ga_2O_3 (b), and γ-Ga_2O_3/α-Ga_2O_3 samples (c) and (d). The nominal γ-Ga_2O_3 contents of the last two were 30% and 60%, respectively. As seen in Fig. 1(a), α-Ga_2O_3 consisted of columnar shaped particles with the length and width of about 1 μm and 0.5 μm, respectively, and each particle was fully crystallized as seen in clear diffraction spots. In contrast, as shown in Fig. 1(b), γ-Ga_2O_3 was composed of aggregates of nm sized fine particles which were not well crystallized giving halo rings without any clear spots of the γ-Ga_2O_3. γ-Ga_2O_3/α-Ga_2O_3 samples (Figs. (c) and (d)) clearly show that fine γ-Ga_2O_3 particles exhibiting a halo ring were deposited on the larger columnar shaped α-Ga_2O_3 particles showing clear diffraction spots. With increasing the γ-Ga_2O_3 content, the coverage of γ-Ga_2O_3 particles over the α-Ga_2O_3 particle increased, but the sizes of the γ-Ga_2O_3 particles were hardly changed. In Fig. 1(d), the α-Ga_2O_3 particle was mostly covered by the γ-Ga_2O_3 particles.

XRD

Fig. 2(a) and (b) show the XRD patterns of γ-Ga_2O_3/α-Ga_2O_3, α-Ga_2O_3, and γ-Ga_2O_3 before and after use for the CO_2 reduction, respectively. Most of the sharp peaks were attributed to α-Ga_2O_3, whereas those attributed to γ-Ga_2O_3 were broad, indicating that the α-Ga_2O_3 is well crystallized, while the γ-

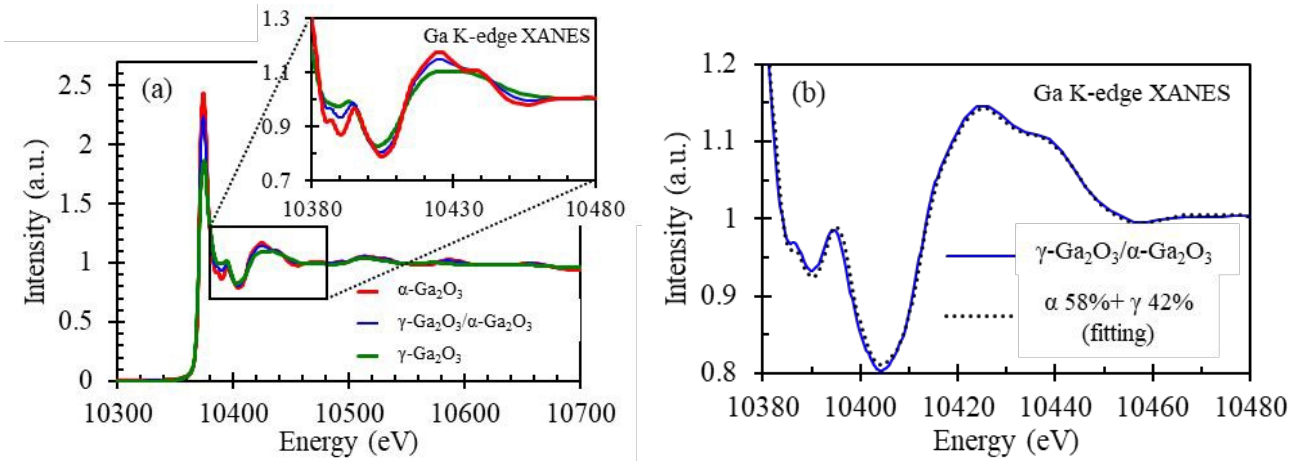

Fig. 3 (a)Ga K-edge XANES spectra of α-Ga_2O_3, γ-Ga_2O_3, γ-Ga_2O_3/α-Ga_2O_3 samples. (b) Least square fitting to the observed XANES spectra with a linear combination of the spectra of α-Ga_2O_3(58%) and γ-Ga_2O_3(42%).

View Article Online
DOI: 10.1039/D6LF00085A

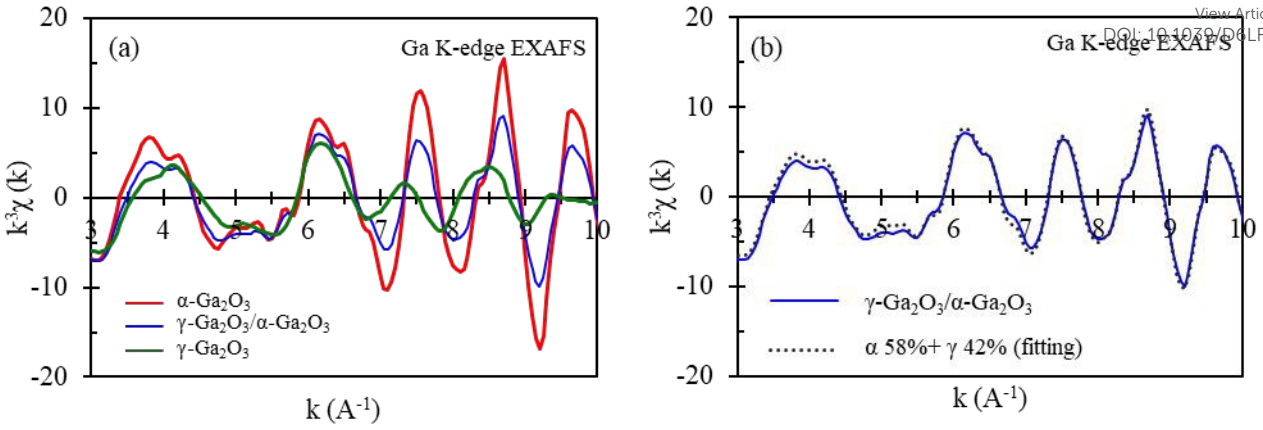

Fig. 4 (a)Ga K-edge EXAFS spectra of α-Ga_2O_3, γ-Ga_2O_3, γ-Ga_2O_3/α-Ga_2O_3 samples. (b) Least square fitting to the observed EXAFS spectra with a linear combination of the spectra of α-Ga_2O_3(58%) and γ-Ga_2O_3(42%).

Ga_2O_3 is poorly crystallized. This corresponds well to the diffraction patterns appeared in Fig. 1. For γ-Ga_2O_3/α-Ga_2O_3, the sharp peaks of α-Ga_2O_3 and the broad peaks of γ-Ga_2O_3 were overlapped. Thus, γ-Ga_2O_3/α-Ga_2O_3 consisting of poorly-crystallized fine γ-Ga_2O_3 particles supported by a larger size fully-crystallized α-Ga_2O_3 particles were synthesized.

As indicated in Fig.2(b), new peaks appeared in the XRD patterns of the samples after use were attributed to GaOOH. This suggests that the surfaces of Ga_2O_3 particles after use were covered by GaOOH. Such hydro-oxidation of the surface of Ga_2O_3 used as a photocatalyst for CO_2 reduction was reported in previous works [9,10].

XAFS

Fig. 3(a) presents the Ga K-edge XANES spectra of α-Ga_2O_3, γ-Ga_2O_3, and γ-Ga_2O_3/α-Ga_2O_3. The differences in XANES fine structures among them were appreciable in the energy range of 10380-10480 eV as shown in the enlarged inset. This allowed us to determine the γ-Ga_2O_3 content of the samples with the linear combination fitting of the XANES spectra as described below. Fig. 3(b) shows an example of the fitting. The fitted spectrum well reproduces the experimental spectrum, giving the compositions of α-Ga_2O_3 and γ-Ga_2O_3 phases of 58% and 42%, respectively.

Fig. 4(a) presents Ga K-edge EXAFS spectra of α-Ga_2O_3, γ-Ga_2O_3, and γ-Ga_2O_3/α-Ga_2O_3 showing clear differences in amplitude and periodicity among the three. This made us to apply the linear combination fitting used in XANES analysis to determine the γ-Ga_2O_3 contents. Fig. 4(b) shows an example of the fitting with the compositions of α-Ga_2O_3 and γ-Ga_2O_3 phases of 58% and 42%, respectively.

In Table 1, thus determined γ-Ga_2O_3 contents by the XANES and EXAFS analyses are compared with the nominal γ-Ga_2O_3 contents calculated by the mixing ratio of reagents for the synthesis. The determined values agreed within a difference of 3% for all samples.

BET specific surface area

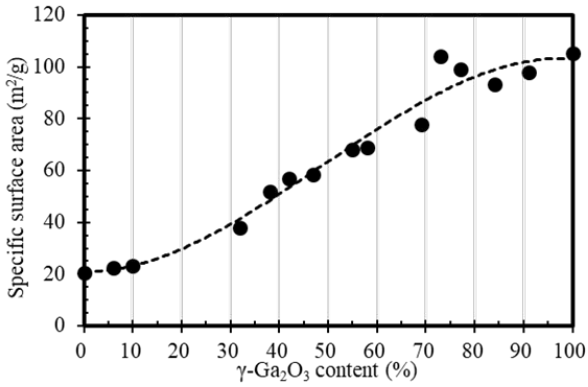

Fig. 5 Changes of BET specific surface area with γ-Ga_2O_3 contents (Dashed line is drawn as a guide to the eyes)

Table 1 Comparison of the γ-Ga_2O_3 contents determined by the least square fitting using XANES and EXAFS spectra and the nominal ones determined for all γ-Ga_2O_3/α-Ga_2O_3 samples.

Amount of charge γ (%)		10	20	30	40	50	53	56	60	70	80	83	86	90
Measured γ	XANES (%)	6	10	32	38	42	47	55	58	69	73	77	84	91
	EXAFS (%)	6	10	31	35	43	47	52	55	68	75	79	83	93

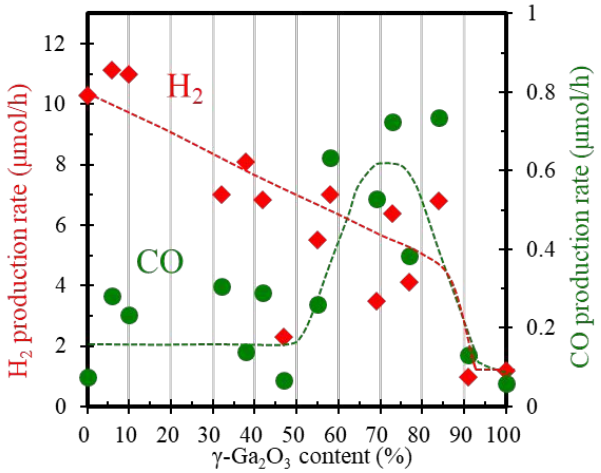

Fig. 6 Production rates of H_2 and CO plotted against the γ-Ga_2O_3 contents of the γ-Ga_2O_3/α-Ga_2O_3 (Dashed line is drawn as a guide to the eyes)

Fig. 5 shows the specific surface areas (SSA) of all samples determined by the BET method as a function of the γ-Ga_2O_3 contents determined by XANES analysis. γ-Ga_2O_3 exhibited much larger SSA than that of α-Ga_2O_3. This is quite reasonable considering the poor crystallinity of the γ-Ga_2O_3. SSA of γ-Ga_2O_3/α-Ga_2O_3 increased with an S-shaped curve showing a slower SSA increase at the lower γ-Ga_2O_3 contents, a roughly linear increase in the middle range, and the saturation over 70% of the γ-Ga_2O_3 content. This is different from the linear increase of SSA with the γ-Ga_2O_3 contents for the mixed phases of α-Ga_2O_3 and γ-Ga_2O_3 observed in the previous work.[10]

This S-shaped SSA increase corresponds well to the TEM observation. At the low γ-Ga_2O_3 contents, nano-sized γ-Ga_2O_3 particles were deposited discretely without appreciable increase of SSA. In the middle range of the γ-Ga_2O_3 contents, both SSA and the coverage of the γ-Ga_2O_3 particles, which have a much larger SSA than that of the α-Ga_2O_3 particles, increased linearly until the surface of the α-Ga_2O_3 particles was mostly covered over 70% of the γ-Ga_2O_3 content.

Photocatalytic reduction of CO_2 with water

The reaction products were mostly H_2, CO, and O_2 for all samples. In Fig. 6 are plotted the production rates of H_2 and CO against the γ-Ga_2O_3 contents of the samples. The H_2 production rate was highest for α-Ga_2O_3 and decreased monotonously with increasing the γ-Ga_2O_3 content. This is quite consistent with our previous work using the mixed phases of α-Ga_2O_3 and γ-Ga_2O_3 and confirms that the H_2 production is dominated on α-Ga_2O_3. The CO production rates stayed small for lower γ-Ga_2O_3 contents, reached a maximum for samples containing 60%-80% of γ-Ga_2O_3, and then decreased markedly for higher γ-Ga_2O_3 contents. This indicates that CO production is promoted by the γ-Ga_2O_3, and the existence of the α-Ga_2O_3 is necessary, i.e. without α-Ga_2O_3, γ-Ga_2O_3 alone showed little activity on the photocatalytic CO_2 reduction with water.

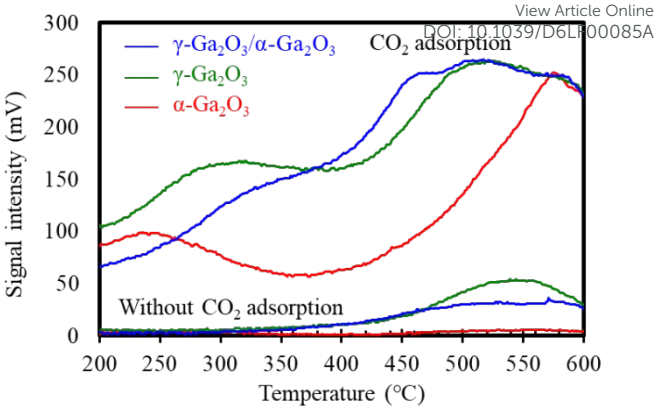

Fig. 7 CO_2-TPD profiles for α-Ga_2O_3, γ-Ga_2O_3 and γ-Ga_2O_3/α-Ga_2O_3 (γ=77%) samples

CO_2-TPD

Fig. 7 shows the CO_2-TPD profiles of α-Ga_2O_3, γ-Ga_2O_3, and γ-Ga_2O_3/α-Ga_2O_3(γ=77 %) in the temperature range from 200°C to 600°C. Although a desorption peak caused by the adsorbed water appeared under 200°C, it was not shown in the figure. The adsorbed amounts of CO_2 on γ-Ga_2O_3 and γ-Ga_2O_3/α-Ga_2O_3 were similar and significantly larger than that on α-Ga_2O_3. This indicates that CO_2 adsorption on γ-Ga_2O_3/α-Ga_2O_3 was mostly originated from γ-Ga_2O_3.

Considering that CO_2 adsorbed on Ga_2O_3 is known to take mainly two species of carbonate and bicarbonate [13], the two dominant peaks appeared at around 200-300°C and 400-500°C could be attributed to the former and the latter, respectively. This agrees with the previous reports showing that as the precursor of CO formation, the bicarbonate desorbing at higher temperature are more favorable than the carbonate [13-15]. The bicarbonate should be formed through the interaction of CO_2 with OH species on the Ga_2O_3 surface. As depicted in Fig. 2(b), the surface of γ-Ga_2O_3 was converted to GaOOH, which very likely enhanced CO_2 adsorption as the bicarbonate (See (1)).

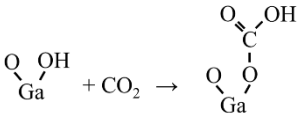

(1)

Discussion

Reaction mechanism

Here, we discuss the mechanism of the photocatalytic CO_2 reduction with water on γ-Ga_2O_3/α-Ga_2O_3. As seen in Fig. 6, H_2 production was dominated on α-Ga_2O_3, while CO production rates increased with the γ-Ga_2O_3 contents and reached a maximum for the samples containing 60-80% of the γ-Ga_2O_3 contents. This observation is quite consistent with the previous work using the mixed phases of α-Ga_2O_3 and γ-Ga_2O_3 [10]. Considering the mechanism suggested in the previous work [10], we have claimed a little more detailed mechanism as follows.

View Article Online DOI: 10.1039/D6LI00085A

I. the surfaces of the α-Ga_2O_3 and γ-Ga_2O_3 particles are hydro-oxidated to GaOOH in water,

$$Ga_2O_3 + H_2O \rightarrow 2GaOOH$$

and GaOOH on γ-Ga_2O_3 particles absorbs CO_2 a bicarbonate.

II. GaOOH on α-Ga_2O_3 is photo-decomposed to α-Ga_2O_3 producing H, as reported by Aoki *et al.* [9],

$$2GaOOH + h\nu \rightarrow \alpha\text{-}Ga_2O_3 + 2H + O \quad (3)$$

III. thus produced H migrates to the γ-Ga_2O_3 particles and reduces the absorbed bicarbonate resulting CO. (This process is not clear to be photo-assisted or not.)

and

IV. without photons, the surfaces of α-Ga_2O_3 and γ-Ga_2O_3 return to their initial states of GaOOH and bicarbonate absorbing state, respectively.

This mechanism is schematically illustrated in Fig. 8.

Effect of sample morphology on the reaction rate

Although the present results are quite similar to those observed in the previous work using the mixed phases of α-Ga_2O_3 and γ-Ga_2O_3, the present production rates of H_2 and CO were clearly smaller. As seen in Fig. 5, SSA showed the S-shaped increase with the γ-Ga_2O_3 contents, while the linear increase was observed in the previous work. This seems reasonable considering the morphology difference that the γ-Ga_2O_3 particles covered the α-Ga_2O_3 particles in the present work, while α-Ga_2O_3 and γ-Ga_2O_3 particles were mixed in the previous work. The CO production rates of both works were hardly correlated to SSA. This also supports the reaction mechanism described above.

In the present work, the γ-Ga_2O_3 content giving the maximum production rate of CO was around 70%, which was clearly higher than 40% of the previous work, while 0.8 mmol · h^{-1} · g^{-1} of the former was clearly less than 3 mmol · h^{-1} · g^{-1} of the latter. This difference could be attributed to the difference in morphology between the supported γ-Ga_2O_3/α-Ga_2O_3 and the mixed phases of α-Ga_2O_3 and γ-Ga_2O_3. Since, in the former, the γ-Ga_2O_3 particles cover the α-Ga_2O_3 columnar particle, the surface area of the α particles was less compared to that of the latter, resulting in less H production and consequently less CO production. In addition, in lower γ-Ga_2O_3 content samples of the former, the γ-Ga_2O_3 particles covered the α-Ga_2O_3 columnar particles rather discretely. Hence, H produced on the α-Ga_2O_3 particle should migrate a longer distance compared to the mixed phase samples, resulting in less CO production.

There is another geometrical factor. In the mixed phases of α-Ga_2O_3 and γ-Ga_2O_3 samples, both phases are directly exposed to the UV light, whereas in the supported γ-Ga_2O_3/α-Ga_2O_3 photocatalyst, the α-Ga_2O_3 particles are partially or fully covered by the γ-Ga_2O_3 particles. In addition, owing to the smaller band gap of the γ-Ga_2O_3, the γ-Ga_2O_3 particles covering the α-Ga_2O_3 particles would shield the UV light from the α-Ga_2O_3 particle beneath [16-18], and thus reduce the H formation on the α-Ga_2O_3 particles and consequently lead to lower CO production. These morphological effects further support the proposed reaction mechanism and emphasize the importance of phase arrangement and morphology in determining photocatalytic performance.

Conclusions

In this work, γ-Ga_2O_3 supported by α-Ga_2O_3 (γ-Ga_2O_3/α-Ga_2O_3) photocatalysts with different γ-Ga_2O_3 contents were synthesized by impregnation followed by calcination. TEM and XRD analysis showed that nano-sized γ-Ga_2O_3 particles were deposited on the surface of columnar shaped α-Ga_2O_3 particles. The γ-Ga_2O_3 content was successfully determined by Ga K-edge XAFS analysis.

Photocatalytic CO_2 reduction with water was carried out to investigate the change of H_2 and CO production rates with the γ-Ga_2O_3 contents. The H_2 production rate decreased with the γ-Ga_2O_3 content, whereas the CO production rate reached a maximum at 60%-80% of the γ-Ga_2O_3 content. These results indicate that H_2 production is dominated on α-Ga_2O_3, while CO production is promoted on γ-Ga_2O_3, which absorbs much larger amount of CO_2 in the form of bicarbonate compared to α-Ga_2O_3. The changes of the production rates of CO and H_2 with the γ-Ga_2O_3 contents are consistent with the previous work using the mixed phases of α-Ga_2O_3 and γ-Ga_2O_3 as photocatalysts. Based on the previously suggested mechanism, a little more detailed mechanism is given as follows : (1) the surface of α-Ga_2O_3 and γ-Ga_2O_3 particles are hydro-oxidated to GaOOH in water and GaOOH on the γ-Ga_2O_3 particles absorb CO_2 as bicarbonate , (2) GaOOH on α-Ga_2O_3 is photo-decomposed to α-Ga_2O_3 producing

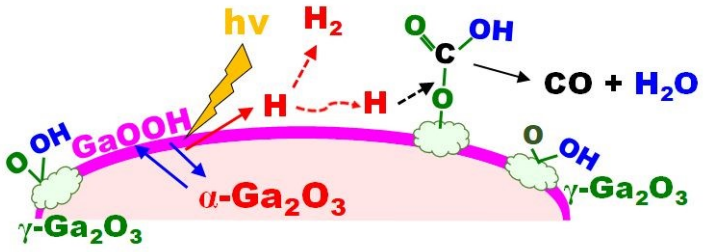

Fig. 8 Schematic drawing of the mechanism of photocatalytic CO_2 reduction with water on γ-Ga_2O_3/α-Ga_2O_3

H, (3) the produced H migrates to the γ-Ga_2O_3 particles and reduces the adsorbed bicarbonate to CO. Without UV-photon, the surfaces of α-Ga_2O_3 and γ-Ga_2O_3 return to their initial states of GaOOH and bicarbonate absorbing state, respectively, and (4) without UV-photon, the surface of α-Ga_2O_3 and γ-Ga_2O_3 return to GaOOH and bicarbonate absorbing state, respectively. Still the detailed pathways of the CO production are unclear and need further research work.

Compared with the mixed phases of α-Ga_2O_3 and γ-Ga_2O_3 photocatalyst reported in the previous study, both H_2 and CO production rates of γ-Ga_2O_3/α-Ga_2O_3 in the present study were lower. This difference is successfully attributed to the difference in the morphology, i.e. g-Ga_2O_3 particles covered the α-Ga_2O_3 particle in the latter, while the mixed phases of α-Ga_2O_3 and γ-Ga_2O_3 particles in the former. These results demonstrate that not only phase composition but also the spatial arrangement of α and γ-Ga_2O_3 plays a crucial role in controlling the CO_2 reduction activity of Ga_2O_3-based photocatalysts.

Conflicts of interest

The authors declare no conflict of interest

Data availability

Raw data were generated at Nagoya University. Derived data supporting the findings of this study are available from Tomoko Yoshida on request.

Acknowledgements

This work was supported by JST, CREST Grant Number JP24031877 and JSPS KAKENHI Grant Number JP20KK0116, Japan.

Notes and references

1 M. Yamamoto, T. Yoshida, N. Yamamoto, T. Nomoto, Y. Yamamoto, S. Yagi and H. Yoshida, *J. Mater. Chem. A* **3** 16810 (2015)
2 N. Yamamoto, T. Yoshida, S. Yagi, Z. Like, T. Mizutani, S. Ogawa, H. Namiki and H. Yoshida, *E-j. surf. sci. nanotechnol.* **12** 263 (2014)
3 Y. Kawaguchi, M. Akatsuka, M. Yamamoto, K. Yoshioka, A. Ozawa, Y. Kato and T. Yoshida, *J. Photochem. Photobiol. A: Chemistry* **358** 459 (2018)
4 K. Yoshioka, M. Yamamoto, T. Tanabe and T. Yoshida, *E-j. surf. sci. nanotechnol.* **18** 168 (2020)
5 M. Yamamoto, S. Yagi and T. Yoshida, *Catalysis Today* **303** 334 (2018)
6 Y. Pan, Z. Sun, H. Cong, Y. Men, S. Xin, J. Song and S. Yu, *Nano Res*. **9** 1689 (2016)
7 S. Kikkawa, K. Teramura, H. Asakura, S. Hosokawa and T. Tanaka, *J. Phys. Chem. C* **122** 21132 (2018)
8 H. Yoon, J. Yang, S. Park, C. Rhee and Y. Sohn, *Appl. Surf. Sci.* **536** 147753 (2021)
9 T. Aoki, M. Yamamoto, T. Tanabe and T. Yoshida, *New J. Chem.* **46** 3207 (2022)
View Article Online
DOI: 10.1039/D6LF00085A
10 N. Ota, Y. Takashiro, M. Yamamoto, T. Tanabe and T. Yoshida, *J. Mater. Chem. A* **13** 6663 (2025)
11 M. Akatsuka, Y. Kawaguchi, R. Itoh, A. Ozawa, M. Yamamoto, T. Tanabe and T. Yoshida, *Appl. Catal. B Environ*. **262** 118247 (2020)
12 L. Li, W. Wei and M. Behrens, *Solid State Sci*.**14** 971 (2012)
13 B. Zhao, Y. Pan and C. Liu *Catalysis Today* **194** 60 (2012)
14 K. Teramura, K. Hori, Y. Terao, Z. Huang, S. Iguchi, Z. Wang, H. Asakura, S. Hosokawa and T. Tanaka, *J. Phys. Chem. C* **121** 8711 (2017)
15 Y. Wang, Y. Sun, X. Liu and F. Dong, *PNAS Nexus* **3** 339 (2024)
16 J. Lyons, ECS *J. Solid State Sci. Technol*. **8** 3226 (2019)
17 T. Oshima, T. Nakazono, A. Mukai and A. Ohtomo, *Journal of Crystal Growth* **359** 60(2012)
18 D.Shinohara and S. Fujita*, Jpn. J. Appl. Phys.* **47** 7311(2008)

View Article Online
DOI: 10.1039/D6LF00085A

Raw data were generated at Nagoya University. Derived data supporting the findings of this study are available from Tomoko Yoshida on request.